



A Shockless Plate-Impact Spalling Technique, Based on Wavy-Machined Flyer-Plates, to Evaluate the Strain-Rate Sensitivity of Ceramic Tensile Strength

M. Dargaud¹ · P. Forquin¹

Received: 26 December 2020 / Accepted: 11 August 2021 / Published online: 10 September 2021
© Society for Experimental Mechanics, Inc 2021

Abstract

Silicon carbide ceramics are widely used for armor protection due to their high compressive strength, high hardness and low density. In the present study, an experimental technique based on the plate-impact technique is developed to measure the tensile strength of ceramic materials. As the strength of ceramics under dynamic loading is highly sensitive to the strain rate, the effort was made to maintain a constant strain rate loading at the failure location. Numerical simulations were used to design several geometries of wavy-machined flyer-plates, which generate a pulse-shaped compressive wave upon impact, with smoothed rising and falling times ranged from 0.65 to 1 μ s. Such shockless plate-impact experiments were performed on a SiC ceramic at impact velocities set between 200 and 450 m/s. Thanks to laser interferometry analysis, the target rear face velocity provides a measurement of the material spall strength at a given strain-rate loading. The strain rate in the failure zone was evaluated via elasto-plastic numerical simulations, using the pulse loading and spall strength determined experimentally. With an appropriate design of the flyer-plate, the plate-impact technique is found to properly allow a well-controlled strain-rate loading around 10^4 – 10^5 s⁻¹ with relatively long rising time to be reached. This work is expected to provide a suitable tool to investigate the high strain-rate behavior of ceramic materials.

Keywords SiC ceramic · Spall strength · Strain-rate sensitivity · Shockless plate impact · Pulse-shaper

Introduction

Silicon carbide (SiC) is an advanced ceramic material extensively studied and developed to address a wide range of applications. To mention a few, SiC is used for abrasive machining [1], electronic systems [2], fluids filtration [3], structural parts requiring high temperature and dimensional stability [4] and lightweight armors [5]. Various sintering routes can lead to dense SiC materials, the most commonly used to reach superior mechanical properties are the solid state pressureless sintering and hot pressed sintering. The high compressive strength (Uniaxial compression strength about 7 GPa [6] and HEL of 13–16 GPa for SiC in solid state sintering [7, 8]), high hardness and relatively low density (3.21 g/cm³) of silicon carbide make it highly suitable to

withstand dynamic loading [9]. For these combined properties, SiC-based materials have been widely investigated to be part of vehicle or body armor protections [10]. Under such extreme loading conditions, the ceramic plate needs to be combined to a metallic or composite backing. The resulting bi-layer system takes profit from the ceramic hardness, to erode the projectile and reduce its perforating power, and the backing ductility, to absorb the residual kinetic energy and contain the fragments [11]. In the wake of the incident compression wave, tensile stresses develop in the target and cause the ceramic intense brittle fragmentation due to the lack of plastic deformation [12].

The damage evolution under dynamic loading is directly related to the nucleation of micro-cracks on the microstructural defects (pores, inclusions, sintering defects, heterogeneities, grain boundaries) [13, 14]. Therefore, the inherent performance of a ceramic-based armor systems relies in part on the ceramic tensile strength, which is about three to ten times lower than its compressive resistance [6]. For this reason, it is necessary to properly evaluate the ceramic tensile and fragmentation behaviors to design an armor

✉ P. Forquin
pascal.forquin@univ-grenoble-alpes.fr

¹ Université Grenoble Alpes, Laboratoire Sols Solides Structures - Risques (3SR), 38041 Grenoble Cedex 9, France

system. With this objective, the Brittle CODEX Chair has been launched and developed at the Laboratoire 3SR. This research program aims at investigating the strain-rate sensitivity of brittle materials in order to improve their modelling at high loading rates [15].

Several classical experimental techniques, such as the Brazilian test [16, 17] or the split Hopkinson (Kolsky) pressure bar (SHPB) [18, 19], enable the resistance of brittle materials having a relatively low dynamic spall strength (concrete, rock, ice, etc.) to be determined. However, to draw any conclusions from SHPB experiments, the sample usually needs to be in a static equilibrium during the test. This means that the loading time (related to the strain rate) has to be well above the round-trip time of the one-dimensional wave in the specimen. Thus, the strain rate is limited by the equation [20]:

$$\frac{\epsilon_{failure}}{\dot{\epsilon}} \gg \frac{2L}{C_{wave}} \quad (1)$$

Classical values for ceramic materials are about 10^{-3} for the tensile failure strain $\epsilon_{failure}$ (the ceramic tensile strength being about one thousandth of their Young's modulus), 10000–12000 m/s for the wave speed C_{wave} . Therefore, considering five round-trips of the wave in the specimen of length L (about 20–30 mm), to prevent any wave dispersion, the use of the Hopkinson pressure bar technique for ceramic tensile characterisation would be limited to very low strain rates of about 40–60 s^{-1} . Above this threshold the specimen is clearly in an unbalanced state, thus leading to possible misinterpretation of the experimental data. Moreover, this technique hardly allows a homogeneous stress to be reached in the cylindrical specimen due to the influence of lateral edges, as the loading time is relatively long (about 20–30 μs) with respect to the small size of the sample.

A more suitable technique to investigate the tensile behavior of ceramic materials at higher strain rate is the plate-impact experiment. Most commonly used to evaluate the dynamic compressive strength of ceramics, the planar impact technique consists in impacting the studied specimen with a thin and flat flyer plate in order to generate a shock loading, with an intensity high enough to cause its failure. Such an impact configuration provides an uni-axial strain state in the material. To be used for tensile characterisation, this technique needs to be performed at relatively low impact velocities to prevent any compression-induced damage to interfere with the tensile response of the material [21]. In such a test, compressive waves are generated upon the dynamic planar impact and propagate through the flyer and target plates. The interaction between the two released waves from the rear free-surfaces of both plates induces a tensile loading in the specimen [22], which can cause its spall failure.

For some brittle materials, such as concrete, micro-concrete and ultra-high performance concrete, it has been experimentally shown that their spall strength is strain rate sensitive, above a threshold value (about $10 s^{-1}$). This was demonstrated by making some adaptations of the SHPB technique to reach strain-rates ranges from 30 to $150 s^{-1}$ [23–26]. Such adaptations are not sufficient for ceramic materials mainly due to their higher strain rate transition, above which their tensile strength is sensitive to the applied strain-rate. Based on thermodynamic energy conditions, Grady gave criteria to relate the spall strength of brittle solids to the strain rate $\dot{\epsilon}$ [9, 27]:

$$\sigma_{spall} = (3\rho C_0 K_c^2 \dot{\epsilon})^{\frac{1}{3}} \quad (2)$$

where ρ is the density, K_c the critical intensity factor and C_0 the bulk velocity ($C_0 = \sqrt{B_0/\rho}$ with B_0 the bulk modulus). The material is considered to follow the relation given in Eq. (2) above a certain strain rate threshold and the Griffith criterion below this value. From micro-mechanical modeling, Denoual, Forquin and Hild related this transition to the material Weibull modulus, crack propagation velocity and the volume considered [28, 29]. They estimated this transition at about $2500 s^{-1}$ with Monte-Carlo simulations in a volume of $1.25 mm^3$ of SiC-100 ceramic. Their approach justifies such a strain-rate dependency of brittle material strength with the competition between microcrack initiation and mesocrack propagation generating obscuration volumes. From this, the material presents a transition from single fragmentation (the whole volume is obscured by a single crack) to multiple fragmentation (the whole volume is obscured by a large number of cracks), according to the applied loading rate.

Despite, these clear demonstrations of the strain rate sensitivity of ceramic behavior, in most experimental studies available in the literature, the dynamic strength of the ceramic is not correlated to the strain rate but only to the impact loading [30]. The spall strength of SiC materials, sintered and hot pressed, is found to increase with the impact loading, up to a threshold stress-loading, above which the spall strength decreases. For instance, Bartkowshi et al. conducted spalling experiments, via planar plate-impact, on a sintered SiC material and found that the spall strength increases with the impact velocity for an impact stress below 3.7 GPa, and decreases above this threshold value [31]. Martin performed the same type of experiments on the same pressureless sintering SiC as the one studied in the present paper, named Hexoloy SA[®], at stress levels below and above the HEL of 13.8 GPa [8]. He observed the same trend for the spall strength evolution according to the impact stress, with a stress threshold around 5–7 GPa. Some authors explain such a behavior by a prior damage generated under compression loading, due to plastic deformation, resulting in a lower

resistance of the material under tensile loading [32]. Grady does not relate this phenomenon by a prior damage under compression, but under decompression. Therefore, responsible for a reverse shear yield before reaching the tensile axial stress, the material decompression would be at the origin of a material loss of cohesion above a certain impact level [9].

However in all these studies, no information is given on the strain rate level reached in the spall plane [31]. The main reason for this is the difficulty of imposing the strain rate during a plate-impact experiment, as it requires to smooth the loading pulse [33]. A solution to overcome this experimental complexity is to design a test in which the strain rate is tailored and maintained constant in the specimen during its spall failure. Mastering the level strain-rate has been a concern for a long time with split Hopkinson pressure bar (SHPB) or Kolsky bar techniques [34]. However, during a planar impact experiment, the shock loading (rectangular compressive pulse) induces a discontinuity of pressure, which leads to extreme and uncontrolled strain rate levels in the spall region, in the order of 10^5 – 10^7 s⁻¹ [35]. To avoid this issue, the specimen needs to be slowly loaded by a ramp pulse [33]. To do so, a high-pulsed power generator (GEPI) equipment can be used [36]. In recent studies, this type of experiment was used to perform spall tests on alumina [37] and SiC ceramics [38] at controlled strain rates, therefore providing a better understanding of their dynamic tensile behavior. The GEPI technique consists in transferring an intense pulsed current to a loop-shaped conductive electrode to generate a tailored ramp pressure via the Laplace effect. This pressure is transferred to the ceramic sample put in contact with the electrode. Therefore, rising time of about 0.2–0.5 μs can be reached and the strain rates levels in the specimen are in the order of 10^4 – 10^5 s⁻¹. However, this technique currently presents the main drawbacks of having a rising time limited by the electrodes size (need of large electrodes to reach low magnetic pressure), requiring to adapt the set up to reach different loading rates and being relatively expensive.

In the present study, a way to overcome these limitations is investigated by adapting the planar impact experimental method to achieve a constant strain rate loading as well as uniform tensile stress state in the spall area. Few studies already investigated shockless plate-impact by using graded-density flyer plates, with a mixed composition (Al–Cu, Mg–Cu for instance) manufactured via 3D printing, tape casting or plasma spray [39, 40]. But this solution presents the limitations of manufacturing cost and quality (uniformity, stability, reproducibility of the complex layered microstructure) and a difficult design via numerical simulations. Moreover, in most of the cases, even if a linearly ramping loading is achieved, the initial pressure shock is not avoided [41]. Early stage studies have been playing on the flyer surface shape to transfer a smoothed tailored ramp to

the ceramic target upon plate-impact [42]. The works found in the literature always include a complex flyer-geometry and expensive manufacturing processes. The technique proposed in the present work focuses on an easy surface design of a metallic flyer plate, with an homogeneous composition, to reach a controlled strain rate in the ceramic sample [43]. Numerical simulations were used as a way to evaluate the required wavy-shaped geometry of the flyer plate and estimate the strain rate level reached in the spall region. Experimental test are performed using the gas gun of 3SR Laboratoire based in Grenoble (France). The spall strengths experimentally obtained for given strain rates are compared to results from GEPI tests found in the literature on the same SiC ceramic [38].

Principle of Spalling Test Based on Shockless Plate-Impact

Upon plate-impact, two compression stress-waves are generated at the contact between the flyer-plate and the target, propagate in opposite directions through both materials and reflect at the free surfaces. The overlap of the corresponding release waves brings the material into a state of tensile stress. If the tensile stress exceeds a critical strength value for the material, the sample undergoes a tensile damage. Moreover, if the loading duration is long enough, cracks propagate in the material and coalesce, thus leading to the spall fracturing. The duration of the compressive pulse and the location of the spall plane can be adjusted by playing on the material of the flyer plate (on which depends the wave speed) and the relative thicknesses of the projectile and target. Ideally the failure should happen in the mid-plane of the tested ceramic tile. The spall failure in the sample can be detected on the profile of the target free-surface particle velocity, measured by laser interferometry. The difference between the maximum velocity and the minimum rebound velocity, called pullback velocity Δv_{pb} , is used to calculate the material spall strength, assuming a linear elastic behavior for the material before reaching the tensile ultimate strength [44]:

$$\sigma_{spall} = \frac{1}{2} \rho_t C_t \Delta v_{pb} \quad (3)$$

where $\rho_t C_t$ is the acoustic impedance of the ceramic, defined as the product of the target density and longitudinal wave speed.

The main issue of this classical plate-impact technique is the discontinuous change in pressure. The planar shock wave leads to uncontrolled loading-rates. The compression rising and falling edges need to be tailored to prevent any shock from generating a pressure discontinuity. The wave diagrams presented in Fig. 1 show the stress state in a specimen with

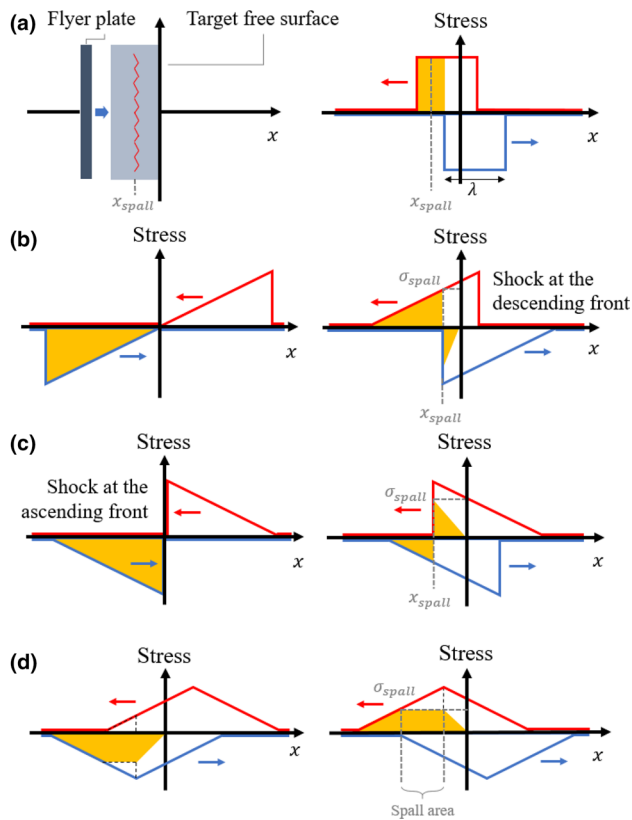


Fig. 1 **a** Plate-impact configuration and corresponding wave diagram with a rectangular compressive wave. **b** Wave diagram for a compressive wave with a smoothed rising edge and sharp descending edge. **c** Wave diagram for a compressive wave with a sharp rising edge and smoothed descending edge. **d** Wave diagram with isosceles triangular pulse-shaped incident wave

a linear elastic material response, according to the shape of the applied compressive wave to the target. The vertical axis corresponds to the free surface of the impacted specimen ($x = 0$). The incident compression wave and reflected tensile waves are colored in blue and red, respectively, and the orange area shows the stress state in the target ($x \leq 0$) resulting from the overlap of both waves. First, in Fig. 1a is shown how a compression wave with sharp rising and falling edges leads to a jump of stress from compression state to tensile state at a given position ($x_{spall} = -\lambda/2$) in the material. Same discontinuity are obtained with a smooth rising edge and sharp falling edge or a smooth falling ramp but sharp rising edge, respectively in Fig. 1b and c. In addition, in both cases (Fig. 1b and c), the spall stress is suddenly reached in a single location of abscissa x_{spall} . In order to completely avoid any jump of stress, both rising and falling edges of the wave need to be smoothed. Furthermore, having a triangular-shaped compressive wave with the same rising and falling edges (Fig. 1d) can provide a constant stress-rate and homogeneous stress field in the material “spall area”. Therefore, a constant and controlled strain rate can be reached in the

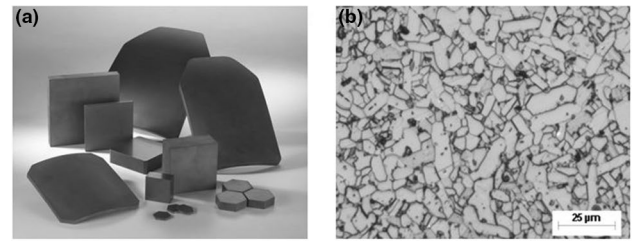


Fig. 2 **a** Saint-Gobain products in Hexoloy SA® [45]. **b** SEM image ($\times 100$) of Hexoloy SA® microstructure [8]

material by mastering the rising and falling edges of the compressive pulse. In addition, the expected stress-rate in the spall area corresponds to the sum of stress-rates of the incident compression wave (falling edge) and the reflected tensile wave (rising edge):

$$\dot{\sigma}_{spall} = \dot{\sigma}_{falling-incident} + \dot{\sigma}_{rising-reflected} \quad (4)$$

For this reason, the main goal of the present study is to design a plate-impact experiment in which the compressive wave transferred to the ceramic upon impact is shaped as a triangular pulse in order to impose the desired loading rate to the tested material.

Materials and Testing Configuration

Materials

Ceramic Target Material

In the present study, a commercial silicon carbide (SiC) grade produced by Saint-Gobain was used as target material. Examples of torso plates made of this material are presented in Fig. 2a. Named Hexoloy SA®, this ceramic is manufactured from the solid state pressureless sintering of submicron SiC alpha powders at temperatures higher than 2000°C. The resulting material is a dense ceramic with an amount of porosity lower than 1.5 vol%, mainly consisting in sintering defects at the grain boundaries and the presence of residual sintering additives such as carbon and boron carbide. The microstructure presents fine SiC grains sized in the range 4–10 μm, as shown in Fig. 2b. The typical mechanical properties of Hexoloy SA® are presented in Table 1.

The nominal size of the rectangular ceramic tiles used for the spall experiments is 50 × 50 mm², with a thickness of 7 mm. During sample preparation, special attention was paid on both flatness and parallelism of the faces, allowing only a maximum gap of 0.01 mm. No further surface polishing was required for the tests.

Table 1 Properties of Hexoloy SA®

Density (kg/m ³)	3150
Hardness H_{V1} (GPa)	24.3
Young's modulus (GPa)	430
Poisson ratio	0.14
Fracture toughness (MPa·√m)	3.0

Wavy-Machined Flyer Material

Discs of Aluminum alloy 7075 were used as projectile material for the plate-impact tests. The nominal diameter of the flyer plates is 70 mm and its thickness is 2 mm. In order to reach a shockless impact, the classically flat flyer plate used for planar impact is wavy-machined, based on Forquin and Zinzner study [33]. They explained that the contact force at the striker/buffer interface increases continuously during the rising time, until the gap between both contact surfaces vanishes. For this reason, the time interval before the full contact may be approximated as the height of wavy-surface (H) divided by the impact velocity of the striker. To control the shape of the compression pulse, the front face of the projectile needs to be designed. Therefore, numerical simulations have been developed to explore the effects of varying the projectile profile to change the compression pulse transferred to the target upon impact. The four resulting geometries, named GEO1, GEO2, GEO3 and GEO4, are described in the next section of this paper. The choice of flyer plates design was also conditioned by the ability to produce complex shapes at small scales and at a reasonable cost by chip-forming process. X-tomography analysis were conducted to control the geometry of the machined flyer plates, in particular the flatness and parallelism of the wavy faces. Images of the front face and cross section are shown in Fig. 3.

Buffer Material

A disc 70 mm in diameter and 3 mm in thickness, made of a steel with a high elastic limit (about 1000 MPa), was used as a buffer plate. Glued to the front face of the target plate, this buffer aims at smoothing the stress heterogeneity transferred to the target material upon impact. A tolerance of 0.02 mm was given to the manufacturer for the flatness and parallelism of both faces of the buffer plate.

Plate Impact Configuration

Gas Gun System

The dynamic testing facility used for the plate-impact tests is a 12 meters-long single stage gas gun installed in 3SR

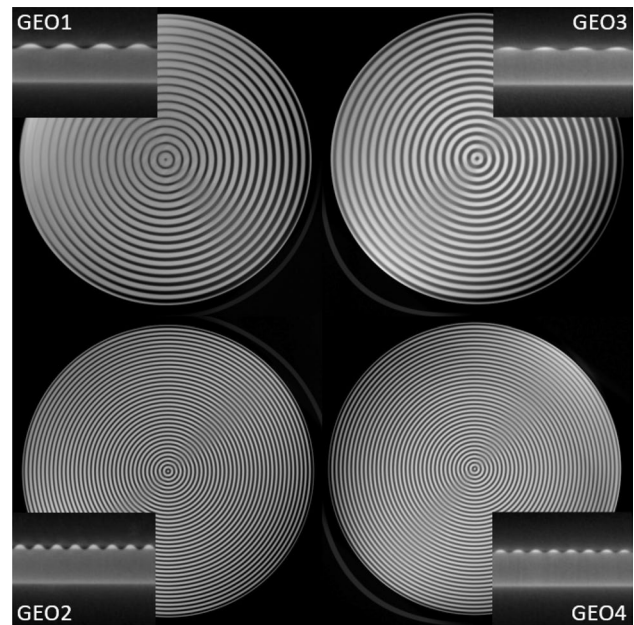


Fig. 3 Images of the flyer plate geometries (GEO1, GEO2, GEO3 and GEO4), extracted from tomography scans (top and cross sections)

Laboratoire (Fig. 4a). The major components are a pressure vessel, a poppet valve, a 6-meter long gun barrel with multiple calibres and a ballistic chamber of 12 m³, in which the target is placed. For this study, experiments were performed using a 80 mm calibre and a striker mass (sabot and flyer plate) of about 400 g, accelerated to an impact speed ranged from 200 to 450 m/s. To reach such impact velocities, compressed Helium is used and the vessel pressure is set in the range 6–34 bars, according to the required velocity. In order to prevent the formation of a shock wave in front of the projectile due to the presence of encapsulated air [46], the ballistic chamber is vacuumed down to 17–25 mbar. The projectile is placed on a polycarbonate (PC) sabot, adjusted to the barrel diameter, Fig. 4b. The software Cesar, from Thiot Ingenierie company, was used to evaluate the gas pressure to be imposed in the pressure vessel to reach the required impact velocity. Input data to predict the

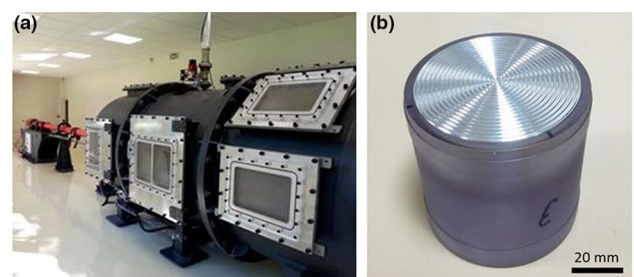


Fig. 4 **a** Multi-caliber Gas gun installed in 3SR Laboratoire. **b** Wavy-machined flyer plate mounted on a PC sabot

striking velocity were the projectile (sabot and flyer plate) weight, the gas pressure and the type of compressed gas used. Two optical barriers placed at the barrel exit end provided an accurate measurement of the projectile velocity at the moment of impact. The tests showed that the velocities obtained were within $\pm 3\%$ of the targeted velocities.

Target Instrumentation and Interferometry System

The ceramic target is mounted on an aluminum disc attached to the launcher tube exit, Fig. 5a. The aluminum support has a circular opening in its center to allow some measurements on the ceramic backface during the dynamic test. The buffer material is stuck to the ceramic front face using an Araldite AY103-1 glue (60 wt.%) combined to a HY951 hardener. A foam layer is placed between the ceramic and its support in order to ensure a full impedance mismatch. In order to prevent any tilt at the projectile/buffer interface during the collision, the target had to be placed perpendicular to the barrel axis. To provide an accurate angular adjustment, the target support is oriented using three nylon screws coupled to Belleville washers. A visible laser, aligned to the barrel, is placed at the entrance of the gas gun and reflects on the buffer surface using a mirror. By playing on the nylon screws, the target was correctly oriented by matching the laser source and its reflection, thus a maximum angular misalignment of 1 mrad was tolerated.

A Photon Doppler Velocimetry (PDV) system is used as the principal diagnostic system for the impact tests [47]. An erbium-doped fiber laser from Keopsys is used as reference source light (wavelength $\lambda = 1550$ nm and power 100 mW) and lights the ceramic backface through a 8 mm-diameter focused optical fiber probe (Oz Optics). This instrumentation is shown in Fig. 5b. Forquin and Zinszner demonstrated from axisymmetric and plane-strain calculations that the same response is obtained in terms of axial stress and particle velocity for various radial positions sufficiently far from the center with respect to the wave period ($> 2P$) and from the edges to avoid lateral released waves [33]. In this

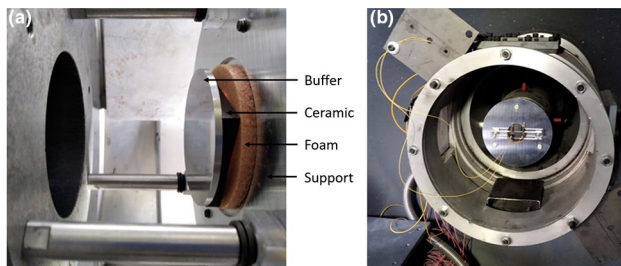


Fig. 5 **a** Top view of the front side of the target system (buffer + ceramic + foam + support) at the launcher tube exit. **b** Picture of the instrumented rear face of the target

range of radial positions, a plane-strain configuration can be considered. Based on these results, an offset distance of 5 mm in the radial direction was imposed between the laser pointer and target center to avoid any measurement error due to the flyer concentric geometry. The tiles were large enough to prevent any edge release waves from interfering with the measurement of the longitudinal wave over the time needed. The light reflected from the measured moving surface, called Doppler-shifted light, is collected by the fiber probe and sent to a home-made detector (provided by CEA Gramat). From the interference between the reflected and reference signals, having different frequencies, the detector generates a signal (in V) which can be recorded on a high-bandwidth oscilloscope (Tektronix DPO 7254 and Keysight DSOS254A). The resulting fringe pattern is directly proportional to the free-surface velocity. As the observed surface moves toward the probe that launches the laser light and collects the shifted return light, the Doppler-shifted frequency is greater than the original laser frequency.

In order to collect a good quality signal, the probe had to be placed perpendicular to the reflecting surface at an initial distance of 20 mm (focal length) [48]. To do so, before any impact test, a function generator is connected to the optical laser and to an oscilloscope to check the shape of the signal, linked to the sample surface quality and the probe/surface relative positions. The electronic device was set to generate a sinusoidal waveform with an amplitude of 1–5 V and a frequency of 1–2 kHz. For any adjustments, the optical fiber is placed in an adjustable PMMA support fixed on the aluminum target support. This preliminary step allows proper positioning of the optical probe with respect to the moving surface (orientation and distance) to capture the best signal possible.

In addition, in all the tests, the velocity of the buffer backside was also measured by using a second optical fiber. To do so, the ceramic target was translated perpendicularly to the impact axis. This configuration with two lasers, recording simultaneously the free-velocity of the buffer and the target, provides the loading pulse transferred to the ceramic for each test. Numerical simulations were used to determine the adequate position of both probes to prevent any boundary effect from interfering with the signal. A drawing represents the target configuration when two optical fibers are used simultaneously (Fig. 6). Thus, the pulse loading induced in the ceramic target could be properly determined and directly implemented in the numerical simulations. This point is further detailed in Sect. 5.1.

Data Recording and Signal Post-Processing

The digitizer was triggered using an optical photodiode. Data were recorded at a sample rate of 10 GS/s (100 ps/pt). The signal was post-processed using a sliding Fourier

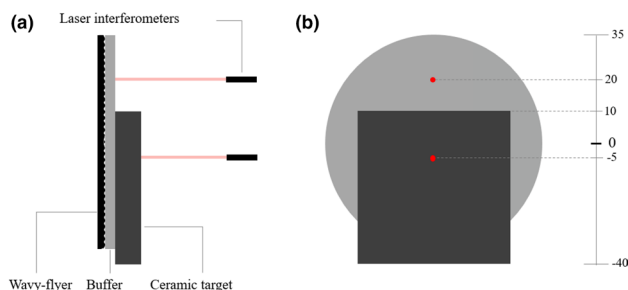


Fig. 6 Schematic showing the 2 laser-probes set-up, used to measure simultaneously the loading pulse and the ceramic free-surface velocity. Cross view (a) and back view (b)

transform method of analysis. The analysis code used is the application WAVE (WAVes data processing for photonic doppler VElocimetry) developed by CEA DAM Gramat, DEA, STEX and LRME. In this way, by recording the beat frequency over time, a complete velocity history of the free surface is obtained.

Elastic Simulations of Shockless Plate-Impact on a Half-Period of the Wavy Flyer Plate

Discretized Geometry and Boundary Conditions

In the present work, in order to minimise the initial shock rise and generate a pulse-shaped wave upon impact, the outer surface of the metallic flyer plate was customized. Based on previous studies [33], the front face of the flyer plate was wavy-shaped to smooth the rising and falling edges of the compressive pulse. By using a Lagrangian x-t diagram, represented in Fig. 7, it is possible to determine the relation between the flyer and target plate thicknesses to obtain a spalling in the median plane of the target :

$$\frac{3L_t}{2C_t} = \frac{2L_p}{C_p} + \frac{L_t}{2C_t} \tag{5}$$

where L and C are respectively the thickness and longitudinal wave speed of the target (t) and projectile (p). Thus, for a flyer plate in aluminum ($C_p \approx 6000$ m/s) and a 7 mm-thick ceramic target ($C_t \approx 12000$ m/s), the projectile needs to be about 2 mm thick. In order to have a linear rising edge, a 'cosine-shape' is given to the front profile of the flyer plate, with a half-period and height, respectively noted P and H. The radius R is defined according to the following equation :

$$R^2 = \left(\frac{P}{2}\right)^2 + \left(R - \frac{H}{2}\right)^2 \tag{6}$$

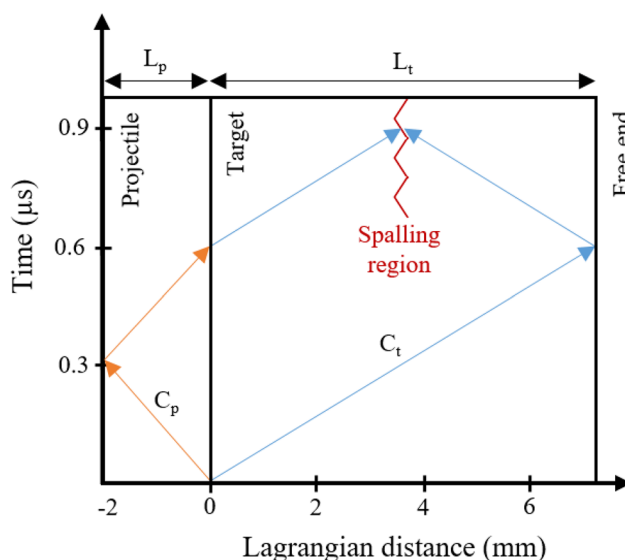


Fig. 7 Lagrangian diagram x-t of a spalling test via plate-impact

First, elasto-plastic numerical simulations were run with the explicit transient dynamic FE method, using the Abaqus/Explicit software. The goal of these preliminary simulations is to evaluate the loading conditions (flyer geometry, flyer material properties and impact velocity) allowing the spalling to happen in the ceramic at a controlled strain rate. C3D8R elements (eight-node hexahedral reduced integration elements) are used to mesh the parts, with an average mesh size of 0.05 mm for the buffer and target. The effect of the flyer mesh size was tested with an average size of 0.05, 0.1 and 0.2 mm. Due to the symmetry and periodicity associated with the problem, only half a period of the wavy flyer plate is discretized, the corresponding part is shown in Fig. 8a. Four geometries for the flyer plate were studied, having a flat rear face and a wavy-shaped front profile with a height (H) and half-period (P) of 0.125–0.25 mm and 0.5–1 mm, respectively, as shown in Fig. 8b. The simulated geometries represent a portion of the target in the Y-X plane with the X-axis being the axis of impact. The normal displacement is set to zero on all nodes of the top/bottom ($u_y = 0$) surfaces of the model (given in Fig. 8a) due to the periodicity of the geometry. The z-axis displacement is set to zero on all the nodes ($u_z = 0$) to traduce the plane strain state for any point located far enough from the target edge and centre. Only one finite element (with a thickness of 1/10 of the period) is considered in the thickness (plane-strain conditions). A surface to surface contact algorithm with only 'hard' normal contact behavior is used to describe the contact between each component (striker/buffer and buffer/target). The flyer plate is given an initial axial velocity, ranged from 200 to 450 m/s. The influence of the projectile behavior on the generated pulse in the ceramic is studies in the next section. The

mechanical behavior of the buffer materials is considered to be elastic perfectly-plastic, as detailed in Table 2. Moreover, as the goal is to evaluate the loading rate generated in the ceramic target before its failure, its behavior is considered elastic, as detailed in the last-mentioned Table 2.

Effect of the Flyer Behavior on the Compressive Stress Pulse

As no mechanical characterisation was performed on the flyer plate material in the present study, the effect of the flyer behavior on the compressive stress pulse was studied via numerical simulations. The influence of the flyer

plate material properties is presented for the configuration of a flyer geometry GEO3 with an impact velocity of 350 m/s. Five different sets of material parameters were considered for the aluminum alloy 7075 to evaluate the effect of the elastic limit, strain hardening behavior, density and Young’s properties. All the material properties are detailed in Table 3.

The average axial stress at the buffer/target interface predicted by considering different material properties of the flyer plate are presented in Fig. 9. It can be noticed that the density (cf. sets of parameters number 2 and 4 in Table 3), elastic limit (cf. sets 1 and 2), strain hardening behavior (cf. sets 2 and 3) do not have a high influence on the compressive

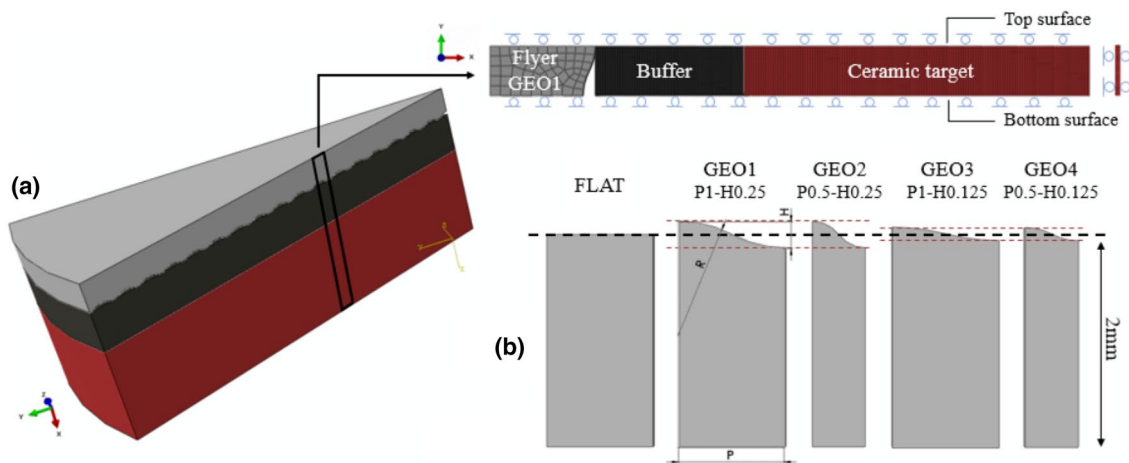


Fig. 8 **a** Slice of the 3D plate-impact configuration and corresponding geometry considering only a single half-period of the wavy flyer plate for the numerical simulations. **b** Sketches of the flat and the four ‘cosine-shaped’ flyer geometries

Table 2 Material elasto-plastic properties considered for the FE calculation

	Material	Thickness (mm)	Density (g/cm ³)	Elastic properties		Plastic yield strength	
				E (GPa)	ν	σ_y (MPa)	ϵ_p
Flyer	Aluminum 7075	2	2.81	71.7	0.33	450	0
Buffer	Steel	3	7.80	200	0.3	1000	0
Target	Hexoloy SA [®]	7	3.15	430	0.14	12000	0
						14000	0.01

Table 3 Sets of material parameters of 7075 aluminium alloy considered for numerical simulations

Behavior	Description	Notations (units)	Sets of numerical values				
			1	2	3	4	5
Elastic	Density	ρ (kg/m ³)	2810	2810	2810	2710	2710
	Young’s modulus	E (GPa)	71.7	71.7	71.7	71.7	64
	Poisson’s ratio	ν	0.33	0.33	0.33	0.33	0.31
Plastic isotropic	Yield stress	R_p 0.2 (MPa)	450	567	567	567	567
	Ultimate strength	R_m (MPa)	–	–	620	–	–
	Elongation	A% (%)	–	–	11	–	–

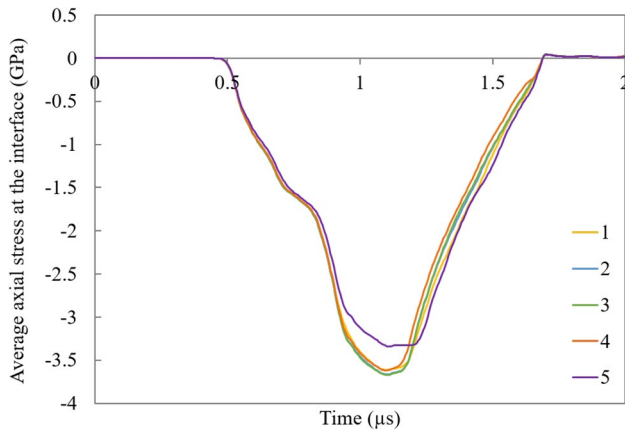


Fig. 9 Effect of the flyer behavior on the shape of the compressive pulse transferred to the ceramic upon plate-impacts, GEO3 350 m/s, from numerical simulations. The sets of numerical parameters for the aluminum alloy (1–5) are given in Table 3

pulse shape. However, increasing the flyer elastic properties (cf. sets 4 and 5) was found to slightly change the compressive pulse shape, as it led to a small increase of the average axial stress magnitude. As a conclusion, the behavior of the flyer plate does not highly influence the shape of the compressive pulse-loading transferred to the ceramic upon the impact of a 'wavy-machined' flyer. Therefore, the flyer metallic part is assumed to have a purely elasto-plastic behavior subsequently, with the set of parameters (1). This assumption is compared to the experimental data in Sect. 5.1.

Pulse-Shaped Compressive Loading

The effect of the flyer profile on the pulse-wave transferred to the target upon impact was explored through numerical simulations. The average axial stress at the buffer/target

interface induced by the different flyer geometries impacting the target at 350 m/s are compared in Fig. 10a. These results confirm that, unlike the flat striker, the wavy geometries generate a compressive wave with smooth rising and falling edges and therefore ensure a shockless impact. The slope of the falling edge is supposed to be mainly linked to the plastic behavior of the aluminum flyer plate, as it is also present for the flat geometry. Increasing the height of the 'cosine-shape' increases the rising time of the compressive wave (0.65 μs for GEO3-4 and 1–1.2 μs for GEO1-2). Varying the impact velocity gives direct control on the magnitude of the average axial stress and on the rising edge of the compressive wave, as shown in Fig. 10b. Moreover, a stress level higher than 500–600 MPa needs to be reached in the SiC ceramic to ensure its spall failure, as it is the estimated dynamic tensile strength of Hexoloy SA[®] at 10^4s^{-1} [38]. Therefore, a combination of flyer-geometry/impact-velocity needs to be found to provide a quasi-triangular pulse. Thus, velocities of about 350–450 m/s were found to be more appropriate for the flyer geometries 3 and 4, whereas lower velocities 150–250 m/s are more suitable for the geometries 1 and 2.

As presented in Fig. 11a for the flyer GEO3 at 350 m/s, the mesh size of the flyer plate (0.05, 0.1 and 0.2 mm) has no effect on the pulse profile. Thus, the choice was made to use a mesh size of 0.2 mm. A 1 mm-thick steel buffer with a high elastic limit was found to be thick enough to homogenise and smooth the stress transferred to the ceramic target, as shown in Fig. 11b. The buffer thickness has no clear effect on the shape of pulse, so a buffer of thickness 3 mm was used for all the tests.

Moreover, the stress profile in the target at different axial positions is given in Fig. 12a for the same impact configuration (GEO3 at 350 m/s). The slope of the compressive wave remains relatively similar in a zone near the target center (elements 3–5), whereas closer to the target front and rear surfaces the pulse is flattened. It can

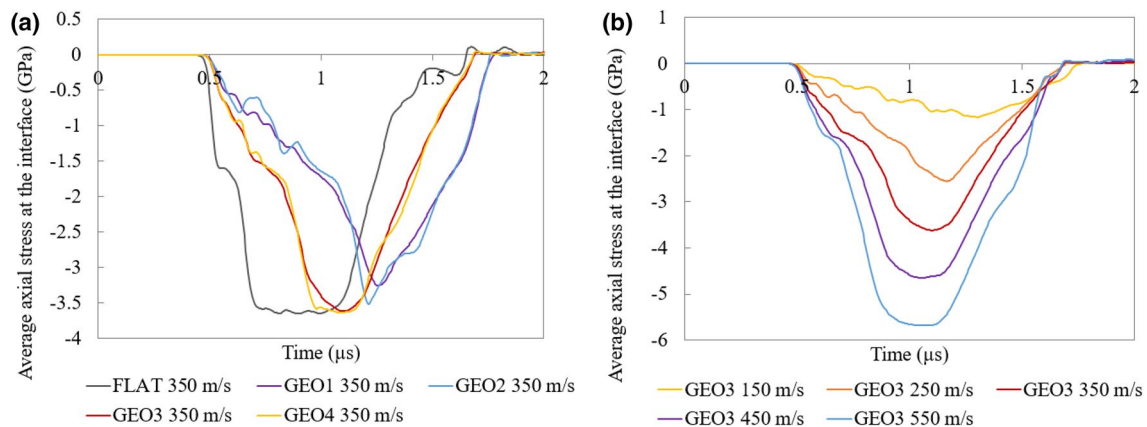


Fig. 10 Effect of the flyer geometry (a) and impact velocity (b) on the shape of the compressive pulse transferred to the ceramic upon plate-impacts, from numerical simulations

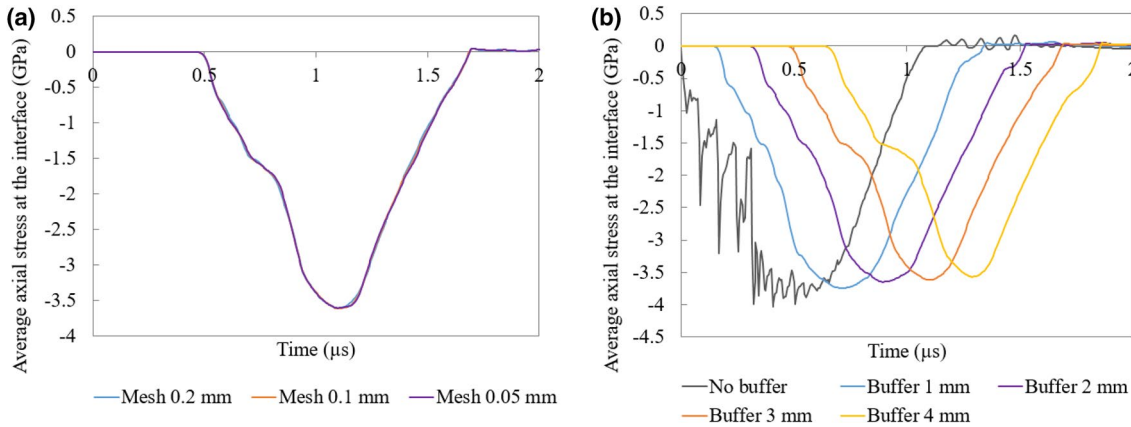


Fig. 11 Effect of the flyer mesh size (a) and buffer thickness (b) on the shape of the compressive pulse transferred to the ceramic, from numerical simulations considering the GEO3 flyer plate impacting the target at 350 m/s

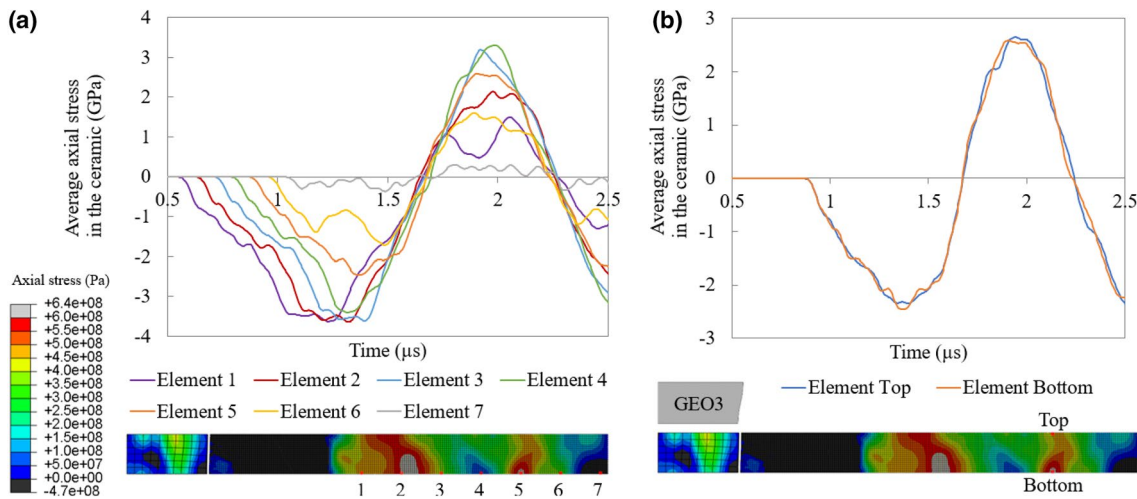


Fig. 12 Axial stress predicted by numerical simulations considering the GEO3 flyer plate impacting the target at 350 m/s and assuming an elastic behavior for the ceramic. **a** Axial stress along the impact direc-

tion. **b** Axial stress in two elements located on the top and bottom sides in the ceramic

be noticed that the loading rate slightly depends on the position of the considered plane, thus, the position of the failure spall plane in the ceramic needs to be properly identify to have an accurate estimation of the strain rate level. A very good homogeneity of stress is shown in Fig. 12b for two elements located at the same axial position but on the top and bottom edges, which means that, in the spall area, the stress and strain-rate can be assumed to be homogeneous along the radial axis (Y-axis) despite the wavy profile of the flyer plate. These results provided confidence in the ability for the four designs to generate a controlled loading rate in the spall region of the target when launched at the proper velocities. Therefore, experiments were performed using this type of flyer plates and

Table 4 Selected nominal configurations for the shockless plate-impact experiments

Flyer geometry	Nominal impact velocities (m/s)		
GEO1	350	-	-
GEO2	-	250	200
GEO3	350	-	-
GEO4	350	450	450

considering impact velocities ranged from 200 to 450 m/s. The nominal configurations chosen to determine the effect of the cosine-shape (H and P) and the impact velocity on the reached strain rate are presented in Table 4.

Experimental Validation of the Flyers Design and Main Spalling Results

Validation of the Generated Pulse from Shockless Plate-Impact Tests

The buffer free-surface velocity profile, obtained from the interferometry post-processing, can be converted in a stress transmitted to the ceramic (assuming a perfectly elastic behavior for the buffer), according to the following equation:

$$\sigma_{transmitted} = \frac{\rho_t C_t * \rho_b C_b}{\rho_t C_t + \rho_b C_b} * v_b \quad (7)$$

with $\rho_b C_b$ the acoustic impedance of the buffer and v_b the buffer free-surface velocity. The obtained stress-time profile was smoothed (using a sliding mean value) and extrapolated (prolonged linearly after the rebound) in view of introducing these data in the numerical simulation. In Fig. 13, the pulse experimentally obtained in the configuration GEO3 353 m/s is compared to pulse predicted by numerical simulation. The numerical pulse was obtained in two different ways. The first one consisted in measuring the average of the axial stress (converted to positive) of each mesh element of the target in direct contact with the buffer and the second one consisted in converting the buffer free-surface velocity profile to a transmitted stress to the ceramic (using Eq. (7)). The very good fit between both curves demonstrates the rightness of using the buffer free-surface velocity to deduce the stress loading

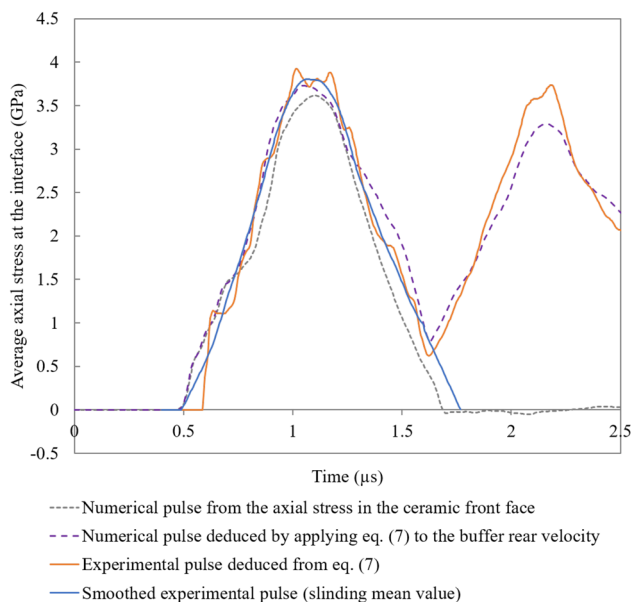


Fig. 13 Comparison of the stress pulse transmitted to the ceramic from experiment and numerical predictions based on an elasto-plastic simulations, for the configuration GEO3 353 m/s. The smoothed experimental pulse is used as an input to evaluate the strain rate

transmitted to the ceramic. This verification is important as, in the next section, the buffer free-surface velocity profile obtained experimentally was converted into a stress input loading for the numerical simulations in order to estimate the strain rate in the spall plane (detailed in Sect. 5.2). In addition, the good match between the experimental and numerical pulses demonstrates the reliability of using simplified elasto-plastic constitutive model for the aluminum alloy to simulate the deformation of the flyer plate.

Moreover, the good match between the numerical stress pulse at the interface buffer/target and the pulse resulting from the buffer free-surface velocity profile converted into a mean axial stress applied to the ceramic validates the following numerical approach to estimate the strain rate (detailed in the next section).

All the tests performed on Hexoloy SA[®] are summarized in Table 5 and the corresponding loading pulse determined experimentally are presented in Fig. 14a. The experimental ceramic free-surface velocity profiles are plot in Fig. 14b and the spall strength estimated from the pullback velocities are detailed in Table 5. The test with the flyer GEO4 at 450 m/s was performed twice to assess the very good repeatability. It can be confirmed that the plate-impact test was pulse-shaped thanks to the use of wavy-machined flyer plates which generate a tailored pulse loading with a various rising time, from 0.65 to 1.2 μ s depending on the flyer geometry/impact velocity combination. Moreover, tests performed with the flyer geometries GEO3 and GEO4 (same cosine height) at the same velocity, provides the exact same loading pulse. Therefore, the cosine-period seems to have no influence on the generated pulse. However, the cosine height and impact velocity have a direct effect on the generated compressive wave. Tests with the geometries GEO1 and GEO2 ($H = 0.25$ mm) at relatively high velocity (360–258 m/s) show a longer rising time compared to GEO3 and GEO4 ($H = 0.125$ mm, 350 m/s). In addition, at the end of the rising edge GEO1_360 and GEO2_258 show a slight stiffening of the rising slope for the buffer and ceramic velocity profiles. Such a behavior results from the fact that at these velocities, the flyer wavy-pattern (having a height of 0.25 mm) was completely flattened before the beginning of the unloading, so the smooth ramp loading started to stiffen before the ceramic failure. Therefore, the impact velocity needs to be kept relatively low for wavy patterns having a high height in order to keep a linear rising edge.

As in most of the studies present in the literature the spall strength of the ceramic is studied with respect to the maximal compression stress reached in the sample, also referred to as 'impact stress', this value is reported in Table 5 for all the tests. This maximal pulse stress σ_{max} was estimated from the maximal velocity V_{max} reached by the target free-surface, according to the following equation:

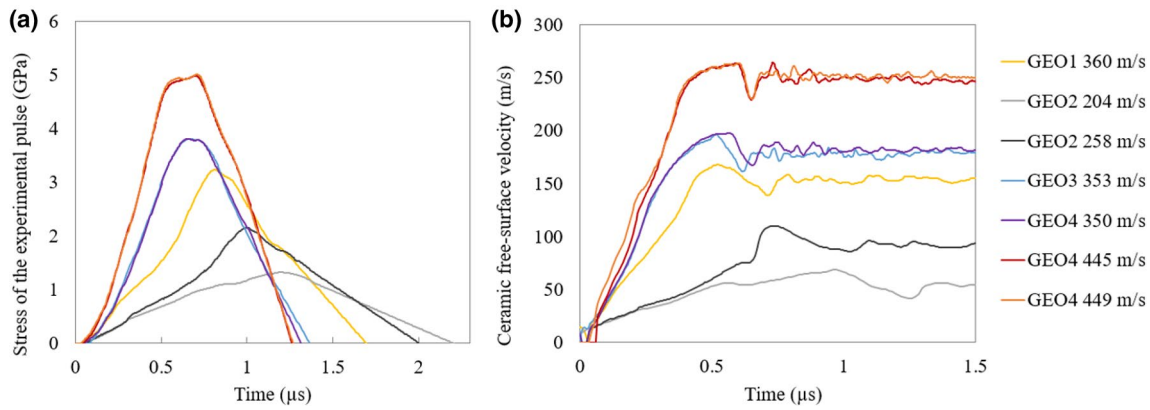


Fig. 14 **a** Experimental velocity profile at the buffer free-surface converted into a stress pulse transferred to the ceramic and **b** experimental free-velocity profile at ceramic free-surface for all the shockless plate-impact tests performed

$$\sigma_{max} = \frac{1}{2} \rho_t C_t V_{max} \tag{8}$$

Moreover, the maximal axial stress reached in the ceramic target during the impact was estimated from the elasto-plastic numerical simulations. It can be noticed that the test with GEO2 at 204 m/s did not provide a high enough stress level in the target (about 230 MPa) to cause its failure. Therefore, the pullback velocity could not be attributed to a spall failure of the ceramic.

Estimation of the Strain Rate at the Spall Location from Elasto-Plastic Numerical Simulations

The strain rate in the failure zone is estimated from elasto-plastic numerical simulations. In order to have a reliable estimation according to the experimental conditions, instead of considering a numerical simulation of the impact between the striker and the target using a half-period of the wavy flyer plate simulations (as in Figs. 8 and 12), the pulse loading obtained experimentally (Fig. 14a) was directly implemented

in the simulation as the input pressure applied to the ceramic target. The spall plane responsible for the measured pullback velocity is assumed to be the plane for which:

- the level of tensile stress reaches the experimental spall strength
- the failure information takes the minimal amount of time to reach the rear face of the ceramic (knowing the longitudinal wave speed of the ceramic material).

Thus, the spall region responsible for the measured pullback can be identified, as shown in Fig. 15a. Then, the strain rate was considered to be the value of axial strain time-derivative in the identify spall plane. In Fig. 15b the axial stress (S11) and strain rate (LE11 derivative) are plot for the configuration with the flyer geometry GEO3 with an impact velocity of 353 m/s. It can be notice that the strain rate is relatively constant during the tensile loading. The margin of error of the strain rate estimation was estimated to about $\pm 1000 \text{ s}^{-1}$, due to the uncertainty on the exact position of the spall failure.

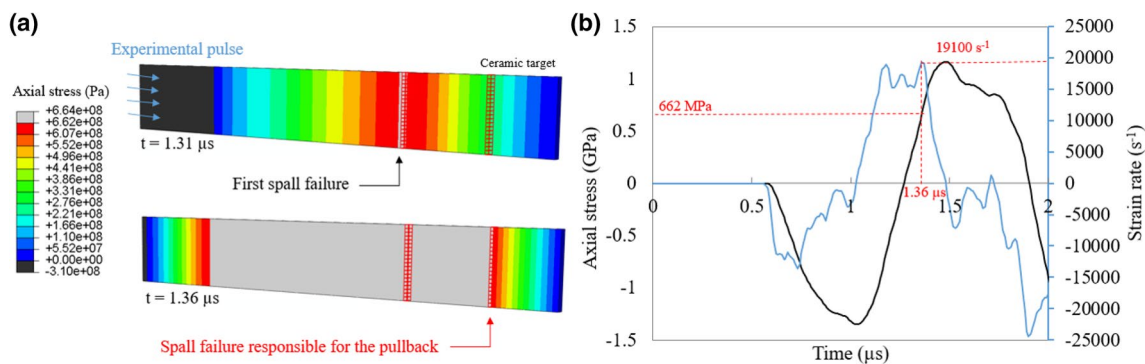


Fig. 15 **a** Identification of the damaged zone responsible for the pullback velocity from elastic numerical simulations on Hexoloy SA[®]. **b** Estimation of the strain rate in the failure area, $\sigma_{spall} = 662 \text{ MPa}$ and $\dot{\epsilon} = 19100 \text{ s}^{-1}$

Comparison with the Results from GEPI Tests

The spall strength results obtained in the present work are compared to the ones measured via the GEPI technique on the same material Hexoloy SA® [38] in Fig. 16 and Table 5. The impact stresses for the GEPI tests, given in Table 5, could be estimated by using the velocity profiles provided by Zinszner et al. in their experimental work [38]. Moreover, they adopted the same methodology as the one described in Sect. 5.2, which combines experimental results and numerical simulations, to evaluate the strain rate during their shockless tests. The only difference is that they used the Denoual-Forquin-Hild (DFH) micro-mechanical model, instead of an elasto-plastic model, to describe the ceramic behavior [28, 29]. Finally, the range of strain rates reached in the present study via the shockless plate impact is comparable to the one of the GEPI experiments (10^4 - 10^5 s⁻¹). The results are in excellent

agreement between both techniques. A clear increase of the ceramic spall strength with an increase of the strain rate can be observed.

The overall method followed in the present paper to evaluate a ceramic spall-strength sensitivity to strain rate is summarized in Fig. 17. This diagram highlights the main steps and corresponding tools, from the design of each experimental configuration by numerical simulations to the data processing of plate-impact experiments. The step of experimental processing consists in characterizing the ceramic spall strength from the measurement of its free-surface velocity upon impact, and estimate the corresponding strain-rate from a numerical simulation where the compression loading pulse is obtained from the buffer free-surface velocity, measured experimentally. Finally this methodology makes possible to ensure a tailored and constant strain rate in the failure zone and to characterize the strain-rate sensitivity of the ceramic tensile strength.

Fig. 16 Comparison of the shockless plate-impact and GEPI results [38] for the strain rate sensitivity of Hexoloy SA® spall strength. The power curve fits the GEPI data

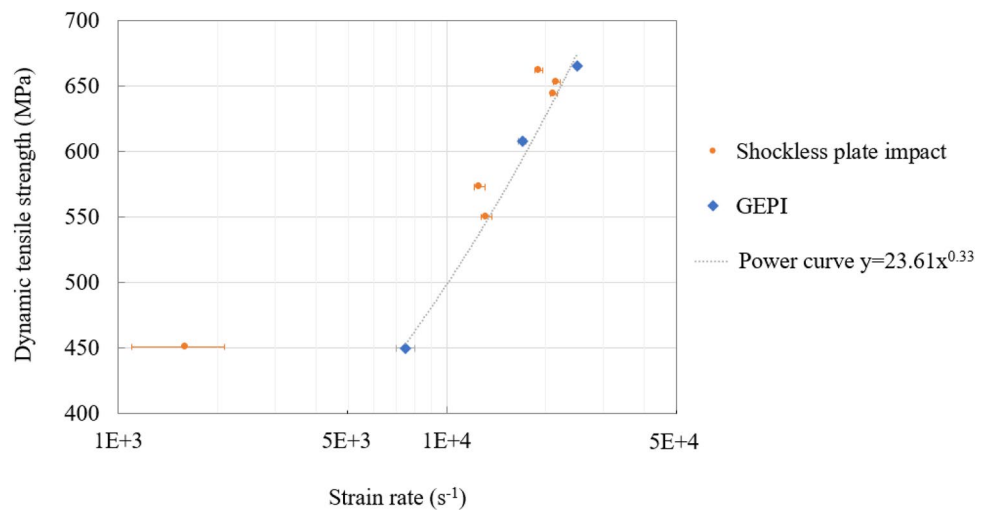


Table 5 List of shockless tests conducted via plate-impact and GEPI techniques on Hexoloy SA®

Experimental Technique	Flyer Geometry	Impact Speed (m/s) (± 3%)	Pulse rising Time (μs) (± 0.1 μs)	Max. pulse Stress (GPa) (± 3%)	Max. reached Stress (GPa)*	Strain rate (s ⁻¹) (± 1000 s ⁻¹)	Spall strength (MPa) (± 3%)
Pulse-shaped plate-impact	GEO1	360	0.8	1.62	0.915	13200	550
	GEO2	204	1.2	1.30	0.230	–	(501)
	GEO2	258	1.0	1.08	0.456	1600	451
	GEO3	353	0.7	1.91	1.162	19100	662
	GEO4	350	0.7	1.91	1.197	12600	573
	GEO4	445	0.65	2.49	1.183	21600	653
	GEO4	449	0.65	2.51	0.910	21200	644
High-pulsed power generator GEPI [38]	–	–	0.5	0.76	–	7500	450
	–	–	0.45	2.84	–	17000	608
	–	–	0.35	5.97	–	25000	665

*From elasto-plastic numerical simulations

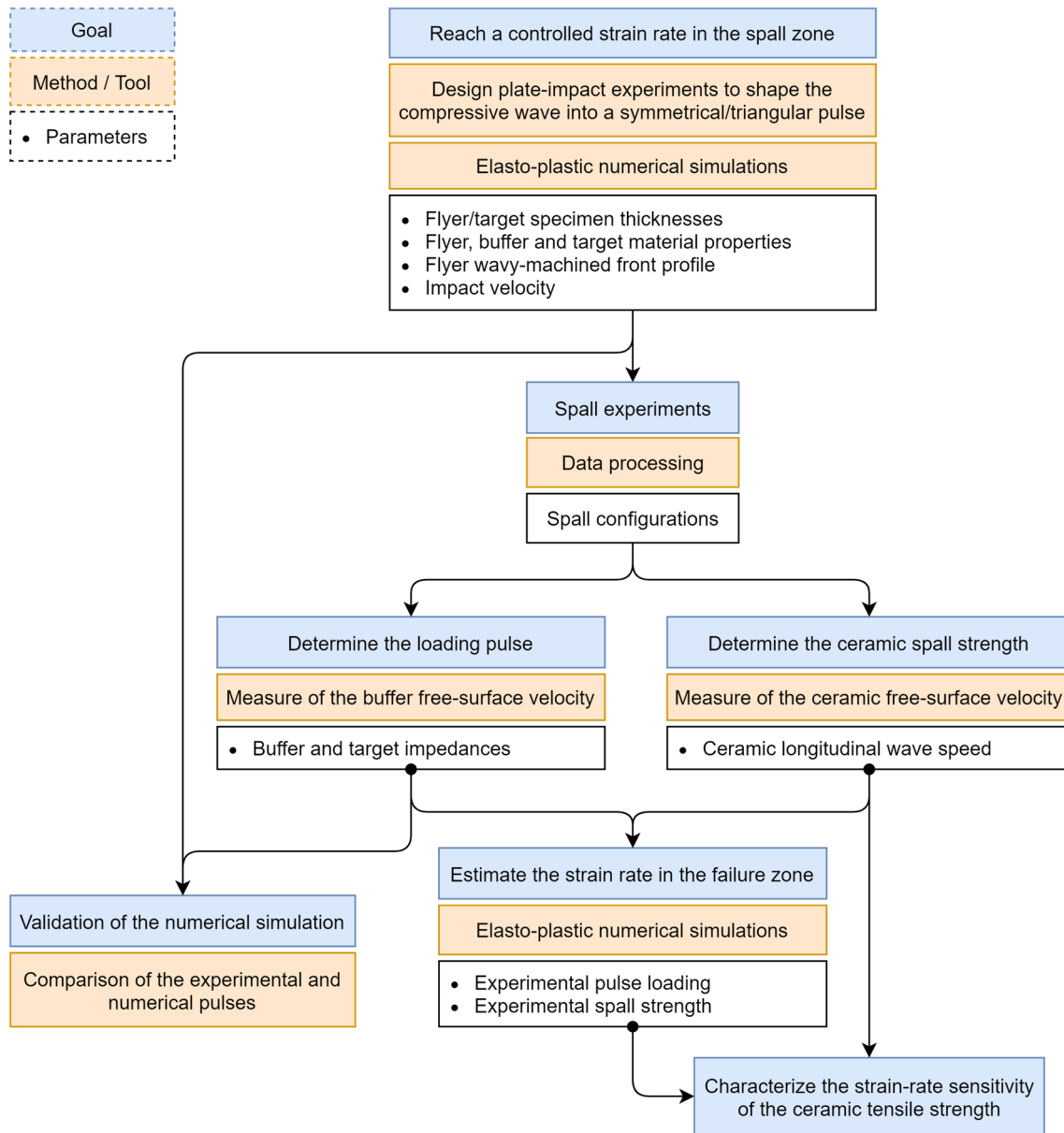


Fig. 17 Diagram summarizing the approach to determine the strain rate sensitivity of ceramic spall strength via shockless plate impact with a wavy-machined flyer-plate

Conclusion

The aim of the present study was to design and perform dynamic spalling tests on ceramic samples at a given strain rate. To do so, the classic planar impact configuration had to be modified, by considering wavy-machined flyer plates, in order to avoid any jump of axial stress and instead maintain a well-controlled loading rate in the specimen failure region. Four geometries of flyer plates were numerically designed by elasto-plastic simulations to control the shape of the loading pulse, according to the flyer geometry, material properties and impact velocity. The preliminary tests

performed on a SiC ceramic gave confidence in the ability to use an aluminum wavy-machined flyer-plate to generate a tailored pulse wave in the target upon a gas gun test. Moreover, the experimental results confirmed that no stress jump was transferred to the ceramic and thanks to the interferometry instrumentation, the spall strength of the SiC ceramic was determined at almost constant strain-rate. The strain rate reached in the ceramic tensile failure location was evaluated through elasto-plastic numerical simulations for each configuration using the loading pulse and spall strength obtained from the shockless experiments. Finally, the ceramic spall strength sensitivity to strain rate could be demonstrated for

strain-rates ranged from 10^4 to 10^5 s⁻¹. The obtained results are in excellent agreement with a previous study using the GEPI technique based on pulsed current.

The subsequent work involves designing other flyer plates to reach a larger range of controlled strain rates (10^5 – 10^6 s⁻¹). Moreover, as initiated by Zinszner and Forquin, such a technique can be extended to the study of the compressive strength sensitivity to loading rate [33]. By this way, a better insight should be given to the development of an accurate modelling of the behavior of armor ceramics, by taking into account their ultimate strength sensitivity to strain rate.

Acknowledgements The authors would like to acknowledge the helpful clarifications obtained from Dr. J.L. Zinszner regarding the interferometry system and data post-processing. For their assistance in preparing the plate-impact experiments, the authors would like to thank W. Kaczmarek, E. Pollier, Dr. L. Zingg and L. Debove. The authors are thankful to Saint-Gobain Research Provence for providing the silicon carbide samples. This research was performed in the framework of the Brittle's CODEX chair, supported by the UGA (Univ. Grenoble Alpes) Foundation and sponsored by the Saint-Gobain and Lafarge-Holcim companies. These sponsors are gratefully acknowledged.

References

- Sheldon DA (1998) Silicon carbide abrasive wheel, US Patent 5,711,774
- She X, Huang AQ, Lucía O, Ozpineci B (2017) Review of silicon carbide power devices and their applications. *IEEE Trans Ind Electron* 64(10):8193–8205
- Hotza D, Di Luccio M, Wilhelm M, Iwamoto Y, Bernard S, da Costa JCD (2020) Silicon carbide filters and porous membranes: a review of processing, properties, performance and application. *J Membr Sci* 610:118193
- Helms HE (1983) Ceramic applications in turbine engines. *Ceramics for high-performance applications III*. Springer, Belin, pp 151–172
- Kuhn M, Tierney D, Simmers M (2016) Silicon carbide for the modern warfighter. *Am Ceram Soc Bull* 96:8
- Forquin P, Denoual C, Cottenot CE, Hild F (2003) Experiments and modelling of the compressive behaviour of two sic ceramics. *Mech Mater* 35(10):987–1002
- Grady DE (1994) Shock-wave strength properties of boron carbide and silicon carbide. *Le J Phys IV* 4(C8):C8-385
- Martin SR (2004) Experimental characterization of the effect of microstructure on the dynamic behavior of SiC. PhD thesis, Georgia Institute of Technology
- Grady DE (1995) Dynamic properties of ceramic materials. Technical report, Sandia National Labs, Albuquerque, NM, USA
- Wilkins ML, Cline CF, Honodel CA (1969) Fourth progress report of light armor program. California University, Livermore. Lawrence Radiation Lab, Technical report
- Crouch IG, Franks GV, Tallon C, Thomas S, Naebe M (2017) Glasses and ceramics. *The science of armour materials*. Elsevier, Amsterdam, pp 331–393
- Zinszner J-L, Forquin P, Rossiquet G (2015) Experimental and numerical analysis of the dynamic fragmentation in a SiC ceramic under impact. *Int J Impact Eng* 76:9–19
- Deng H, Nemat-Nasser S (1992) Dynamic damage evolution in brittle solids. *Mech Mater* 14(2):83–103
- Shockey DA, Curran DR, Seaman L, Rosenberg JT, Petersen CF (1974) Fragmentation of rock under dynamic loads. *Int J Rock Mech Min Sci Geomech* 11:303–317
- Forquin P, Blasone M, Georges D, Dargaud M, Saletti D, Andò E (2020) The brittle's codex chair. *DYMAT Winter School 2020*:180–185
- Lambert DE, Ross CA (2000) Strain rate effects on dynamic fracture and strength. *Int J Impact Eng* 24(10):985–998
- Gálvez F, Rodriguez J, Sánchez V (1997) Tensile strength measurements of ceramic materials at high rates of strain. *Le J Phys IV* 7(C3):C3-151
- Ramesh KT (2008) High rates and impact experiments. *Handb Exp Solid Mech* 933:929–960
- Forquin P, Riedel W, Weerheijm J (2013) Dynamic test devices for analyzing the tensile properties of concrete. *Understanding the tensile properties of concrete*. Elsevier, Amsterdam, pp 137–181
- Forquin P (2017) Brittle materials at high-loading rates: an open area of research. *Philos Trans A Math Phys Eng Sci* 375(2085):20160436
- Paris V, Frage N, Dariel MP, Zaretsky E (2010) The spall strength of silicon carbide and boron carbide ceramics processed by spark plasma sintering. *Int J Impact Eng* 37(11):1092–1099
- Antoun T, Curran D, Razorenov S, Seaman L, Kanel GI, Utkin A (2003) Spall fracture. *Spall fracture: shock wave and high pressure phenomena*. Springer, New York
- Schuler H, Mayrhofer C, Thoma K (2006) Spall experiments for the measurement of the tensile strength and fracture energy of concrete at high strain rates. *Int J Impact Eng* 32(10):1635–1650
- Forquin P, Erzar B (2010) Dynamic fragmentation process in concrete under impact and spalling tests. *Int J Fract* 163(1–2):193–215
- Erzar B, Forquin P (2010) An experimental method to determine the tensile strength of concrete at high rates of strain. *Exp Mech* 50(7):941–955
- Forquin P, Lukić B (2018) On the processing of spalling experiments part i: identification of the dynamic tensile strength of concrete. *J Dyn Behav Mater* 4(1):34–55
- Grady DE (1988) The spall strength of condensed matter. *J Mech Phys Solids* 36(3):353–384
- Forquin P, Hild F (2010) A probabilistic damage model of the dynamic fragmentation process in brittle materials. *Adv Appl Mech* 44:1–72
- Denoual C, Hild F (2000) A damage model for the dynamic fragmentation of brittle solids. *Comput Methods Appl Mech Eng* 183(3–4):247–258
- Dandekar DP, Bartkowski PT (2001) Tensile strengths of silicon carbide (SiC) under shock loading. Technical report, Army Research Lab Aberdeen proving ground MD
- Bartkowski P, Dandekar DP (1996) Spall strengths of sintered and hot pressed silicon carbide. In: *AIP conference proceedings*, vol 370, pp 535–538. American Institute of Physics
- Dandekar DP, Bartkowski PT (2001) Chapter 10. Spall strengths of silicon carbides under shock loading. In: *Meyers MA, Murr LE, Staudhammer KP (eds) Fundamental issues and applications of shock-wave and high strain-rate phenomena*, pp 71–77
- Forquin P, Zinszner J-L (2017) A pulse-shaping technique to investigate the behaviour of brittle materials subjected to plate-impact tests. *Philos Trans R Soc A* 375(2085):20160333
- Forrestal MJ, Warren TL (2021) A conical striker bar to obtain constant true strain rate for Kolsky bar experiments. *J Dyn Behav Mater* 7:161–164
- LaLone BM, Gupta YM (2009) Elastic limit of x-cut quartz under shockless and shock wave compression: Loading rate dependence. *J Appl Phys* 106(5):053526
- Davis JP, Deeney C, Knudson MD, Lemke RW, Pointon TD, Bliss DE (2005) Magnetically driven isentropic compression

- to multimegabar pressures using shaped current pulses on the z accelerator. *Phys Plasmas* 12(5):056310
37. Erzar B, Buzaud E (2012) Shockless spalling damage of alumina ceramic. *Eur Phys J Special Topics* 206:05
 38. Zinszner J-L, Erzar B, Forquin P (2017) Strain rate sensitivity of the tensile strength of two silicon carbides: experimental evidence and micromechanical modelling. *Philos Trans R Soc A* 375:20160167
 39. Yep S, Belof J, Orlikowski D, Nguyen J (2013) Fabrication and application of high impedance graded density impactors in light gas gun experiments. *Rev Sci Instrum* 84:103909
 40. Martin LP, Patterson JR, Orlikowski D, Nguyen JH (2007) Application of tape-cast graded impedance impactors for light-gas gun experiments. *J Appl Phys* 102(2):023507
 41. Hall AC, Battaile CC, Webb EB, Wise JL, Urrea DA, McCloskey JF, Roemer TJ, Beatty DE (2008) Graded-density thermal spray coatings for light gas gun flyer plates. Technical report, Sandia National Lab (SNL-NM), Albuquerque, NM, USA
 42. Cotton M, Chapman D, Winter R, Harris E, Eakins D (2015) Tailored ramp wave generation in gas gun experiments. In: *EPJ Web of Conferences*, vol 94, p 01065. EDP Sciences
 43. Forquin P (2016) Procédé et dispositif pour mesurer la résistance des matériaux solides par impact de plaques sans choc, October 11 . Patent UGA, INPI, N°1000369617
 44. Novikov SA, Divnov II, Ivanov AG (1966) Investigation of the fracture of steel, aluminum and copper during explosive loading. *Fiz Metallov Metalloved* 21(4):608–615
 45. <https://www.ceramicsrefractories.saint-gobain.com/hexoloy/why-use-hexoloy-sic-material>. Saint-Gobain website
 46. Plassard F, Mespoulet J, Hérel PL (2011) Analysis of a single stage compressed gas launcher behaviour: from breech opening to sabot separation. In: 8th European LS-DYNA Users Conference, Strasbourg, 05
 47. Strand OT, Goosman DR, Martinez C, Whitworth TL, Kuhlow WW (2006) Compact system for high-speed velocimetry using heterodyne techniques. *Rev Sci Instrum* 77:083108–083108
 48. Kettenbeil C, Mello M, Bischann M, Ravichandran G (2018) Heterodyne transverse velocimetry for pressure-shear plate impact experiments. *J Appl Phys* 123:125902

Publisher's Note Springer Nature remains neutral with regard to jurisdictional claims in published maps and institutional affiliations.